Synthesis, Crystal Structure and Magnetic Properties of an Iron(III) Pyridine-2,3,5,6-tetracarboxylate Complex

Wei Xu, Jian-Li Lin, Hong-Lin Zhu, Fang-Hong Hu, and Yue-Qing Zheng

Center of Applied Solid State Chemistry Research, Ningbo University, Ningbo, 315211, P. R. China

Reprint requests to Prof. Dr. Yue-Qing Zheng. Fax: Int. +574/87600747.
E-mail: zhengcm@nbu.edu.cn

A new pyridine-2,3,5,6-tetracarboxylato-bridged Fe(III) complex with a K^+ counter ion, $K[Fe(H_2pdtc)_2]$ (**1**), was prepared from the reaction of $Fe_2(SO_4)_3 \cdot 7H_2O$, pyridine-2,3,5,6-tetracarboxylic acid and KOH under ambient conditions. The complex has been characterized by single-crystal and powder X-ray diffraction, IR spectroscopy, TG analysis, elemental analyses, and magnetic measurements. Through intermolecular hydrogen bonding and π-π stacking interactions, the $[Fe(H_2pdtc)_2]^-$ complex anions are assembled into supramolecular double chains with the K^+ cations located between them. The variable temperature magnetic measurement has shown a weak ferromagnetic behavior over the range $300 - 10$ K followed by antiferromagnetic behavior below 10 K.

Key words: Fe(III) Complex, Pyridine-2,3,5,6-tetracarboxylic Acid, Supramolecular Assembly, Magnetic Properties

Introduction

Molecule-based magnetic polymers have attracted intense interest in recent years, due to not only the fundamentals of magnetic interactions and magneto-structural correlations, but also the development of new functional molecule-based materials [1 – 4]. Over the last decades, novel magnets have been developed by the strategy of combing paramagnetic first row transition metals with appropriate bridging ligands. The nature of the bridging ligand is the key to the properties of the material in the solid state since it dictates the sign and magnitude of the magnetic exchange between the paramagnetic metal centers. The design, synthesis and characterization of Fe(II) and Fe(III) complexes with benzene-based multi-carboxylate ligands therefore play a relevant role in the world on magnetic materials [5 – 7]. Compared with benzene multicarboxylic acid, pyridine-2,3,5,6-tetracarboxylic acid, H_4pdtc, is of special interest in the construction of novel coordination polymers, since it can be deprotonated to a different extent to generate a series of ligands such as the H_3pdtc^-, H_2pdtc^{2-}, $Hpdtc^{3-}$, and $pdtc^{4-}$ anions, which exhibit various pH-tunable coordination modes to construct diverse coordination frameworks and supramolecular architectures. Pyridine-2,3,5,6-tetracarboxylate anions also display additional coordination modes because the pyridine ring and two carboxylate groups in the 2- and 6-positions can chelate the metal ions safely to generate stable structures, while the other carboxylate groups on the pyridine ring are able to connect several metal centers to form high-dimensional coordination frameworks. However, to date first row transition metal complexes containing pyridine-2,3,5,6-tetracarboxylate ligands have not been much investigated [8, 9].

As a part of our ongoing systematic investigation of pyridine multi-carboxylic acid complexes [10, 11], herein, we report a new di-protonated pyridine-2,3,5,6-tetracarboxylato-bridged Fe(III) complex with a K^+ counter ion, namely $K[Fe(H_2pdtc)_2]$, which has been fully characterized by crystallographic techniques and magnetic studies. The magnetic behavior of the title compound is discussed by using two approaches, based on (i) the mononuclear Fe(III) ion in a octahedral crystal field and (ii) a dinuclear spin Hamiltonian $H = -2JS_1S_2(S_1 = S_2 = 5/2)$.

Results and Discussion

Syntheses

Under ambient conditions, the reaction of pyridine-2,3,5,6-tetracarboxylic acid (H_4pdtc), $Fe_2(SO_4)_3 \cdot 7H_2O$ and KOH in an aqueous solution yielded

K[Fe(H$_2$pdtc)$_2$]. Slow evaporation of the resulting solution led to the crystallization of the title compound. The phase purity of the crystalline product was confirmed by comparing the experimental powder X-ray diffraction (PXRD) pattern with the corresponding one simulated on the basis of the single-crystal data (Fig. 1), as well as by an elemental analysis. The above synthetic reaction can be expressed by the following equation:

$$Fe_2(SO_4)_3 + 4\,H_4pdtc + 2\,KOH \rightarrow$$
$$2\,K[Fe(H_2pdtc)_2] + 3\,H_2SO_4 + 2\,H_2O$$
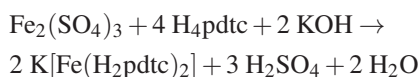
The title compound was found to be stable in air and insoluble in common solvents such as water, ethanol, and acetone.

Description of the crystal structure

The asymmetric unit of the title compound consists of one K$^+$ cation, one Fe^{3+} cation and two di-protonated pyridine-2,3,5,6-tetracarboxylate (H$_2$pdtc)$^{2-}$ anions (namely H$_2$pdtc1 and H$_2$pdtc2, which contain the atoms N1 and N2, respectively) as shown in Fig. 1. The H$_2$pdtc units are both deprotonated at the 2,6-positioned carboxyl groups. The (H$_2$pdtc1)$^{2-}$ anion possesses two strong, nearly linear asymmetric O–H$\cdots$O hydrogen bonds with d(O$\cdots$O) = 2.500(2) and 2.501(2) Å between two adjacent carboxylate groups on both sides of the central pyridyl ring, but has only one intramolecular hydrogen bond with d(O11$\cdots$O10) = 2.457(2) Å. It should be noted that the C(sp^2)–C(sp^2) bond lengths in the C=C–COO$^-$ groups (C1–C6, C5–C9, and C10–C15) are 1.534(2), 1.531(2), and 1.535(2) Å, respectively,
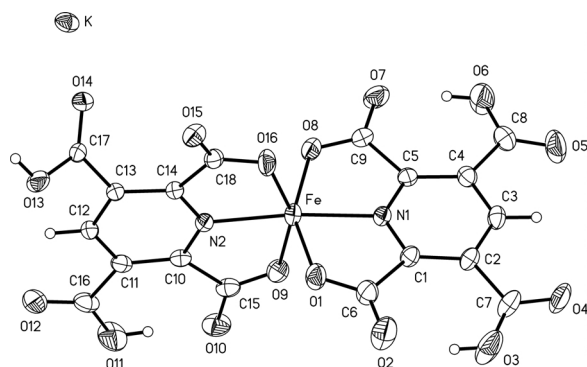

Fig. 1. ORTEP view of the K[Fe(H$_2$pdtc)$_2$] complex with displacement ellipsoids (45 % probability level) and atomic labeling.

Table 1. Selected bond lengths (Å), and angles (deg) for **1** with estimated standard deviations in parentheses[a].

Distances			
Fe–O1	1.994(1)	Fe–O16	1.980(1)
Fe–O8	1.994(1)	Fe–N1	2.092(1)
Fe–O9	2.006(1)	Fe–N2	2.082(1)
Angles			
O1–Fe–O8	151.90(5)	O8–Fe–N2	105.30(6)
O1–Fe–O9	91.87(6)	O9–Fe–O16	151.86(5)
O1–Fe–O16	93.76(6)	O9–Fe–N1	96.70(6)
O1–Fe–N1	76.21(6)	O9–Fe–N2	75.12(5)
O1–Fe–N2	102.79(6)	O16–Fe–N1	111.42(5)
O8–Fe–O9	95.43(6)	O16–Fe–N2	76.74(5)
O8–Fe–O16	92.47(6)	N1–Fe–N2	171.77(5)
O8–Fe–N1	76.01(6)		

Hydrogen bonding contacts					
D–H	d(D–H)	d(H$\cdots$A)	d(D–H$\cdots$A)	$\angle$(D–H$\cdots$A)	A
O3–H3	0.81	1.71	2.500(2)	164	O2
O6–H6	0.84	1.67	2.501(2)	174	O7
O11–H11	0.84	1.62	2.457(2)	171	O10
O13–H13	0.83	1.78	2.591(2)	164	O4$^{\#1}$

[a] Symmetry transformations used to generate equivalent atoms: $^{\#1}$ $x-1, y+1, z$.

which are close to C(sp^3)–C(sp^3) bond lengths [12] and slightly longer than other similar carbon-carbon bonds in (H$_2$pdtc)$^{2-}$ anions and other pyridine carboxylate complexes [8, 11]. This may be caused by the metal-carboxylate coordination. The pyridine rings of the ligands chelating the central Fe atoms are orientated nearly perpendicular to each other (dihedral angle: 85.0(1)°). The values of the dihedral angles between the planes of the carboxylic groups and the pyridine ring plane in the H$_2$pdtc1 ligands are 4.6(4)°, 7.9(3)°, 5.8(3)°, and 1.8(3)°. While the O13–C17–O14 carboxyl group shows a substantial twist with respect to the central pyridyl ring plane with a dihedral angle of 52.7(1)°, the others have corresponding dihedral angles of only 2.7(2)°, 2.0(3)°, and 12.7(3)°, indicating a considerable influence of hydrogen bonding interactions.

Acting as tridentate ligands, the H$_2$pdtc1 and H$_2$pdtc2 anions chelate the Fe atom *via* the two pyridyl N atoms and four O atoms of different carboxylate groups in four five-membered chelate rings to complete a significantly distorted octahedral FeN$_2$O$_4$ unit. Two nitrogen atoms (N1 and N2) and two carboxylate oxygen atoms (O1 and O8) form the equatorial base, while the other two carboxylate oxygen atoms (O9 and O16) occupy the axial positions. The deviation from the ideal octahedral geometry is indicated by the difference in *cisoid* [75.12(5)° – 111.42(5)°] and *transoid* angles [151.86(5)° – 171.77(5)°]. The Fe–O bond lengths fall in the region 1.994(1) to 2.006(1) Å,
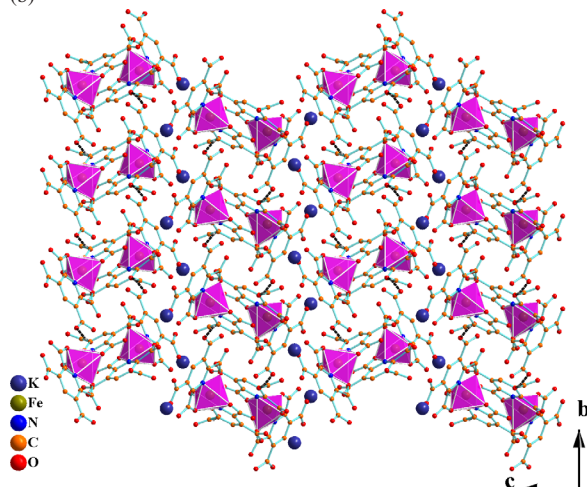
(a)
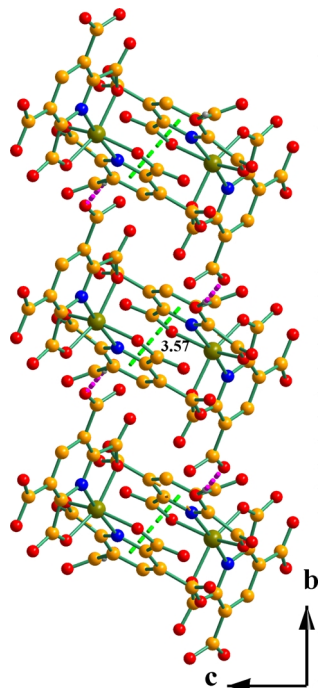
(b)

Fig. 2. (a) Double chains generated from hydrogen bonding and interchain π-π stacking interactions in the title compound; (b) crystal structure of the title complex (the large spheres represent the K^+ ions).

while d(Fe–N) = 2.082(1) and 2.092(1) Å (Table 1). The above structural parameters are all within the normal ranges for Fe(III) centers [13, 14].

The O13 atom donates a hydrogen atom to the carboxylate oxygen atom O4$^{\#1}$ to form an intermolecular hydrogen bond with d(O–H$\cdots$O) = 2.591(2) Å

and $\angle$(O–H$\cdots$O) = 164°. Due to this type of interactions, the $[Fe(H_2pdtc)_2]^-$ complex anions are assembled into supramolecular chains extending along the [010] direction with the H_2pdtc2 ligands parallel to each other. Each H_2pdtc2 ligand of one chain enters a void between two H_2pdtc2 ligands from the adjacent chain. Such interdigitation results in the formation of supramolecular double chains (Fig. 2a). Two neighboring H_2pdtc2 ligands face each other in an antiparallel mode with an interplanar distance of 3.57 Å, indicating significant π-π stacking interactions [15]. The resulting columnar double chains are in turn arranged in the crystal structures according to *pseudo* 1D close-packing patterns (Fig. 2b). The K^+ cations are surrounded by nine O atoms of carboxylate groups with K–O contact distances in the range 2.714(1) – 3.078(1) Å, and are located between the double chains.

Infrared spectra

As illustrated in Fig. 3, the absorption peaks at 1720 and 1690 cm^{-1} are due to the -COOH groups in the complex. The asymmetric stretching vibrations (v_{as}) of the carboxylate groups result in strong absorption bands centered at 1610 and 1560 cm^{-1}, while the medium strength absorption due to the symmetric vibrations (v_s) is observed at 1337 cm^{-1}. The differences $\Delta v_{as-s} = (v(CO_2)_{asym} - v(CO_2)_{sym})$ are 273 and 223 cm^{-1}, corresponding to a monodentate coordination mode of the carboxylate groups [16]. The sharp absorption peaks observed at 1388, 3096 and 746 cm^{-1} can be ascribed to the pyridyl ring and to C-H deformation vibrations. The absorptions in the range 687 – 1054 cm^{-1} can be attributed to the skeleton vibrations of the organic ligand.

Thermal analysis

The thermogravimetric curve (Fig. 3) shows that the title compound decomposes in two steps. It is found to be stable below 290 °C. The observed weight loss for the first step in the range 290 – 485 °C reaches 74.5 % close to the calculated value (74.38 %) for removal of two moles of the pyridine-2,3,5,6-tetracarboxylate ligands. The dehydration thus leads to the formation of an intermediate "$Fe(OH)_3 + 1/2 K_2O$". Upon further heating, the resulting intermediate loses 3/2 equivalents of "H_2O" in the range 590 – 650 °C, and the observed weight loss of 4.8 % corresponds well to the calculated value of 4.5 %. The rufous residue represents 20.7 % in weight and is a mixture of $1/2 Fe_2O_3$ and $1/2 K_2O$.
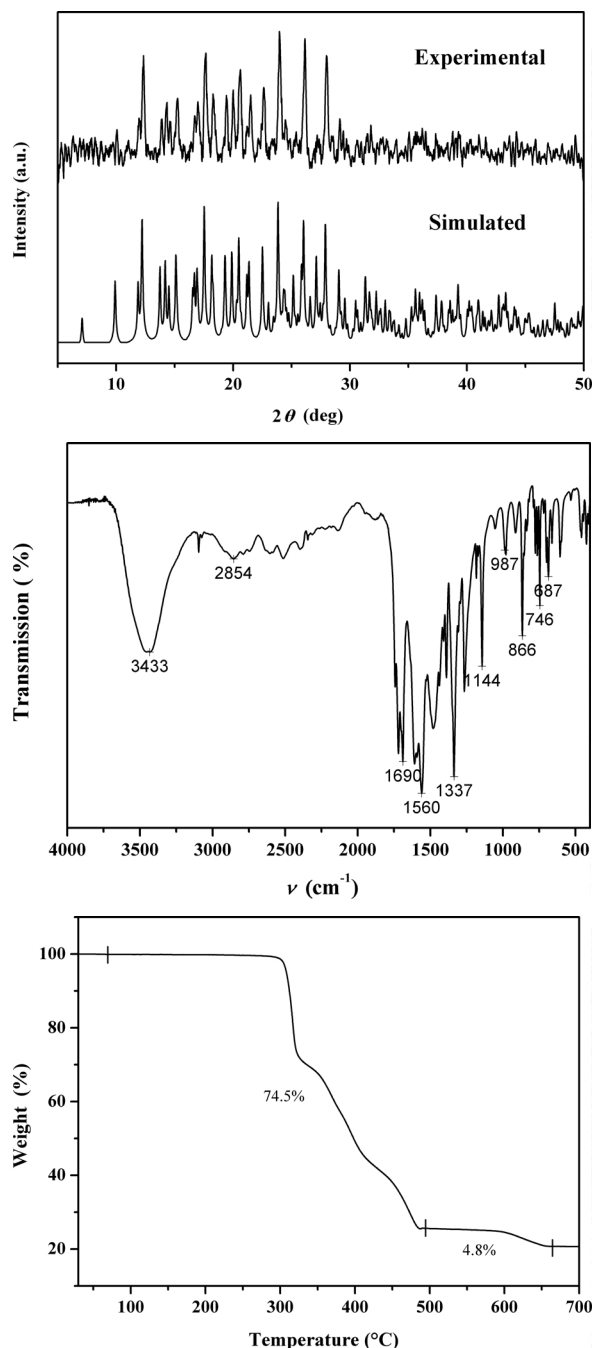
Fig. 3. (top) Experimental and simulated PXRD patters, (middle) infrared spectrum, and (bottom) TG curve for the title compound.

Magnetic properties

The magnetic behavior is presented in the form of χ_m and $\chi_m T$ *versus* T plots (χ_m being the mag-

netic susceptibility per Fe(III) ion at a magentic field of 5 kOe in Fig. 4. For the title compound, the r. t. $\chi_m T$ value of 3.901 $cm^3 \cdot K \cdot mol^{-1}$ is slightly smaller than the spin-only value of 4.375 $cm^3 \cdot K \cdot mol^{-1}$ for high-spin Fe(III) ($S = 5/2$), indicating an unquenched orbital contribution arising from the $^6A_{1g}$ ground state of Fe(III). Upon lowering the temperature, the $\chi_m T$ value smoothly increases until it reaches a maximum value of 4.247 $cm^3 \cdot K \cdot mol^{-1}$ around 10 K and then decreases to 4.219 $cm^3 \cdot K \cdot mol^{-1}$ at 2 K, indicating the presence of ferromagnetic behavior from r. t. to 10 K, then followed by antiferromagnetic behavior below 10 K. This magnetic behavior is discussed in two approaches as follows.

(i) When the title compound is treated as a mononuclear Fe(III) complex, it should be interpreted assuming the D (zero-field splitting parameter) and/or the λ (spin-orbit parameter) in the corresponding formulas. Only when the distortion of the coordination geometry is low, the D and λ parameters can be used simultaneously, but so far, this is impossible to carry out. Thus the experimental data have to be fitted to the formula (Eq. 1) for a $S = 5/2$ mononuclear system with a D parameter [17].

$$\chi_x = \frac{Ng^2\beta^2}{4kT} \frac{9 + 8/x - 11e^{2x}/2x - 5e^{-6x}/2x}{1 + e^{-2x} + e^{-6x}}$$
$$\chi_z = \frac{Ng^2\beta^2}{4kT} \frac{1 + 9e^{-2x} + 25e^{-6x}}{1 + e^{-2x} + e^{-6x}} \tag{1}$$

with $\chi_{mono} = (2\chi_x + \chi_z)/3$ and $x = D/kT$.

Because only a very weak magnetic interaction was expected in the molecular field approximation as zJ', the measured magnetic susceptibility data were fitted to (Eq. 2),

$$\chi_m = \frac{\chi_{mono}}{1 - (2zJ'Ng^2\beta^2)\chi_{mono}} \tag{2}$$

where χ_m is the exchange-coupled magnetic susceptibility actually measured, χ_{mono} is the magnetic susceptibility in the absence of the exchange field, zJ' is the weak molecular interaction exchange parameter, and the rest of the parameters have their usual meanings. The best fit is obtained with values of $g = 2.18$, $|D| = 9.0$ cm^{-1}, $zJ' = -0.04$ cm^{-1}, and the agreement factor $R = 3.9 \times 10^{-4}$ ($R = \sum[(\chi_m)_{obs} - (\chi_m)_{calc}]^2/[(\chi_m)_{obs}]^2$).

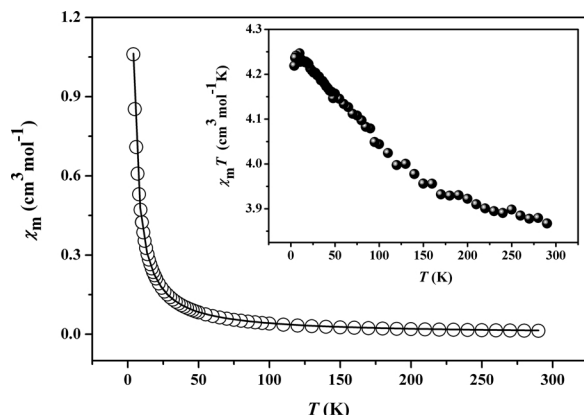(ii) To gain a deeper insight into the nature of the magnetism, the magnetic structure can be represented

Fig. 4. Temperature dependence of the magnetic susceptibility of **1**. Solid lines represent the best fit.

by a dinuclear model connected *via* π-π stacking interactions with the Hamiltonian $H = -2JS_1S_2$ ($S_1 = S_2 = 5/2$), for which the J coupling constant can be applied as shown in Eq. (3) [18, 19]. Owing to the very weak magnetic interactions between the Fe(III) ions, the expression is to be corrected using the molecular field approximation (Eq. 4), to which the measured magnetic susceptibility data are fitted.

$$\chi_{di} = \frac{2Ng^2\beta^2}{kT} \frac{e^x + 5e^{3x} + 14e^{6x} + 30e^{10x} + 55e^{15x}}{1 + 3e^x + 5e^{3x} + 7e^{6x} + 9e^{10x} + 11e^{15x}} \quad (3)$$

where $x = J/kT$.

$$\chi_m = \frac{\chi_{di}}{1 - (2zJ'/Ng^2\beta^2)\chi_{di}} \quad (4)$$

A very satisfactory fit was reached for the data in the whole temperature range 2 – 300 K. The results are $J = 0.22$ cm^{-1}, $g = 1.95$, $zJ' = -0.04$ cm^{-1}, and the agreement factor $R = 3.8 \times 10^{-6}$ ($R = \sum[(\chi_m)_{obs} - (\chi_m)_{calc}]^2/[(\chi_m)_{obs}]^2$). The positive J value indicates that ferromagnetic coupling exists between the Fe(III) ions *via* π-π stacking interactions, and the negative zJ' clearly indicates the existence of very weak antiferromagnetic coupling between the adjacent Fe(III) ions, consistent with the magnetic behavior displayed by the $\chi_m T$ *vs.* T plot in Fig. 4.

Experimental Section

Materials

All chemicals were commercially available in reagent grade and were used without further purification.

Table 2. Crystal structure data for **1**.

Formula	$C_{18}H_6FeKN_2O_{16}$
M_r	601.20
Crystal size, mm^3	$0.43 \times 0.35 \times 0.29$
Crystal system	monoclinic
Space group	$P2_1/c$
a, Å	12.682(3)
b, Å	7.704(2)
c, Å	21.595(4)
β, deg	100.42(3)
V, Å^3	2075.1(8)
Z	4
D_{calcd}, g cm^{-3}	1.92
$\mu(MoK_\alpha)$, cm^{-1}	1.0
$F(000)$, e	1204
hkl range	$\pm16, \pm9, \pm27$
$((\sin\theta)/\lambda)_{max}$, Å^{-1}	0.65
Refl. measured / unique / R_{int}	4707 / 4175 / 0.0252
Param. refined	356
$R(F)$ / $wR(F^2)$[a] (all refl.)	0.0299 / 0.0770
GoF (F^2)[b]	1.002
$\Delta\rho_{fin}$ (max / min), e Å^{-3}	0.35 / −0.45

[a] $R(F) = \Sigma||F_o| - |F_c||/\Sigma|F_o|$, $wR(F^2) = [\Sigma w(F_o^2 - F_c^2)^2/\Sigma w(F_o^2)^2]^{1/2}$, $w = [\sigma^2(F_o^2) + (0.0427P)^2 + 1.0349P]^{-1}$, where $P = (\text{Max}(F_o^2,0) + 2F_c^2)/3$; [b] $\text{GoF} = [\Sigma w(F_o^2 - F_c^2)^2/(n_{obs} - n_{param})]^{1/2}$.

Physical methods

Powder X-ray diffraction measurements were carried out with a Bruker D8 Focus X-ray diffractometer to check the phase purity. The C, H and N microanalyses were performed with a PE 2400II CHNS elemental analyzer. The FT-IR spectrum was recorded from KBr pellets in the range 4000 – 400 cm^{-1} on a Shimadzu FTIR-8900 spectrometer. A thermogravimetric measurement was carried out from r. t. to 700 °C on a preweighed sample using a Seiko Exstar 6000 TG/DTA 6300 apparatus with a heating rate of 10 °C·min^{-1}. Single-crystal X-ray diffraction data were collected on a Rigaku Raxis-Rapid X-ray diffractometer. The temperature-dependent magnetic susceptibility was determined with a Quantum Design SQUID magnetometer (Quantum Design Model MPMS-7) in the temperature range 2 – 300 K with an applied field of 5 kOe.

Synthesis of K[Fe(H$_2$pdtc)$_2$]

An aqueous solution of 0.1055 g (0.20 mmol) Fe$_2$(SO$_4$)$_3 \cdot$ 7 H$_2$O in 5 mL H$_2$O was added to a stirred aqueous solution of 0.2051 g (0.80 mmol) pyridine-2,3,5,6-tetracarboxylic acid in 10 mL H$_2$O. To this mixture 0.8 mL (1.0 M) aqueous KOH was dropwise added, and the resulting blue solution (pH = 2.43) was subsequently allowed to stand at r. t. Slow evaporation for two weeks afforded yellow-green block crystals (yield: 57 % based on the initial Fe$_2$(SO$_4$)$_3 \cdot$ 7H$_2$O input). The crystals were characterized by their IR spectrum (KBr disc): ν = 3433, 3096, 2845, 1720, 1690, 1610, 1560,

1479, 1388, 1337, 1267, 1182, 1144, 1054, 987, 912, 866, 746, 687, 605 cm^{-1}. – $C_{18}H_6FeKN_2O_{16}$ (601.20): calcd. C 35.96, H 1.01, N 4.66; found C 35.74, H 0.80, N 4.52.

X-Ray structure determination

A suitable single crystal was selected under a polarization microscope and fixed with epoxy cement on a fine glass fiber which was then mounted on a Rigaku R-Axis Rapid IP X-ray diffractometer, operated with graphite-monochromatized MoK_α radiation ($\lambda = 0.71073$ Å) for cell determination and subsequent data collection. The reflection intensities in the θ range 3.00 – 27.45° were collected at 295 K using the ω scan technique. The employed single crystal exhibited no detectable decay during the data collection. The data were corrected for *Lp* and empirical absorption effects. The programs SHELXS-97 and SHELXL-97 [20] were used for structure solution and refinement. The structure was solved by using Direct Methods. Subsequent difference Fourier syntheses enabled all non-hydrogen atoms to be located. After several cycles of refinement, hydrogen atoms associated with a carbon atom were geometrically generated, and the rest of the hydrogen atoms were located from the successive difference Fourier syntheses. Finally, all non-hydrogen atoms were refined with anisotropic displacement parameters by the full-matrix least-squares technique, and hydrogen atoms with isotropic displacement parameters set to 1.2 times the values for the associated heavier atoms. Detailed information about the crystal data and structure determination is summarized in Table 2. Selected interatomic distances and angles are tabulated in Table 1.

CCDC 809363 contains the supplementary crystallographic data for this paper. These data can be obtained free of charge from The Cambridge Crystallographic Data Centre *via* www.ccdc.cam.ac.uk/data_request/cif.

[1] D. Gatteschi, R. Sessoli, *Angew. Chem.* **2003**, *115*, 278 – 309; *Angew. Chem. Int. Ed.* **2003**, *42*, 268 – 297.

[2] O. Waldmann, *Coord. Chem. Rev.* **2005**, *249*, 2550 – 2566.

[3] M. Kurmoo, *Chem. Soc. Rev.* **2009**, *38*, 1353 – 1379.

[4] B. Bechlars, D. M. D'Alessandro, D. M. Jenkins, A. T. Lavarone, S. D. Glover, C. P. Kubiak, J. R. Long, *Nature Chem.* **2010**, *2*, 362 – 368.

[5] C. Serre, F. Millange, S. Surblé, J. M. Grenèche, G. Férey, *Chem. Mater.* **2004**, *16*, 2706 – 2711.

[6] N. Hao, E. H. Shen, Y. G. Li, E. B. Wang, C. W. Hu, L. Xu, *Inorg. Chem. Commun.* **2004**, *7*, 131 – 133.

[7] Y. Xu, L. Han, Z. Z. Lin, C. P. Liu, D. Q. Yuan, Y. F. Zhou, M. C. Hong, *Eur. J. Inorg. Chem.* **2004**, 4457 – 4462.

[8] A. H. Yang, H. Zhang, H. L. Gao, W. Q. Zhang, L. He, J. Z. Cui, *Cryst. Growth Des.* **2008**, *8*, 3354 – 3359.

[9] X. J. Sun, J. F. Zhou, M. Z. Yan, *Chin. J. Inorg. Chem.* **2009**, *25*, 1483 – 1486.

[10] X. W. Wang, Y. R. Dong, Y. Q. Zheng, J. Z. Chen, *Cryst. Growth Des.* **2007**, *7*, 613 – 615.

[11] Y. Q. Zheng, W. Xu, H. L. Zhu, J. L. Lin, L. Zhao, Y. R. Dong, *CrystEngComm* **2011**, *13*, 2699 – 2708.

[12] F. H. Allen, O. Kennard, D. G. Watson, L. Brammer, A. G. Orpen, R. Taylor, *J. Chem. Soc., Perkin Trans.* **1987**, S1–S19.

[13] T. J. Mizoguchi, J. Kuzelka, B. Spingler, J. L. DuBois, R. M. Davydov, B. Hedman, K. O. Hodgson, S. J. Lippard, *Inorg. Chem.* **2001**, *40*, 4662 – 4673

[14] N. Bouslimani, N. Clément, G. Rogez, P. Turek, M. Bernard, S. Dagorne, D. Martel, H. N. Cong, R. Welter, *Inorg. Chem.* **2008**, *47* 7623 – 7630

[15] C. Janiak, *J. Chem. Soc., Dalton Trans.* **2000**, 3885 – 3896.

[16] K. Nakamoto, *Infrared and Raman Spectra of Inorganic and Coordination Compounds*, 4th ed., Interscience-Wiley, New York, **1986**.

[17] O. Kahn, *Molecular magnetism*, VCH Publisher, New York, **1993**.

[18] X. Feng, J. G. Wang, C. Z. Xie, N. Ma, *Z. Anorg. Allg. Chem.* **2007**, *633*, 2085 – 2088.

[19] B. Zhang, Y. Zhang, M. Kurmoo, *Inorg. Chim. Acta* **2007**, *360*, 2513 – 2517

[20] G. M. Sheldrick, SHELXS/L-97, Programs for Crystal Structure Determination, University of Göttingen, Göttingen (Germany) **1997**. See also: G. M. Sheldrick, *Acta Crystallogr.* **1990**, *A46*, 467 – 473; *ibid.* **2008**, *A64*, 112 – 122.